Effect of Hydrogen-Bond Networks in Controlling Reduction Potentials in *Desulfovibrio vulgaris* (Hildenborough) Cytochrome c_3 Probed by Site-Specific Mutagenesis†

Carlos A. Salgueiro,‡,§ Patrícia N. da Costa,‡ David L. Turner,‡,|| Ana C. Messias,‡,⊥ Walter M. A. M. van Dongen,▽ Lígia M. Saraiva,‡ and António V. Xavier*,‡

Instituto de Tecnologia Química e Biológica, Universidade Nova de Lisboa, Rua da Quinta Grande 6, 2780-156 Oeiras, Portugal, Departamento de Química da Faculdade Ciências e Tecnologia da Universidade Nova de Lisboa, Quinta da Torre, 2829-516 Caparica, Portugal, Department of Chemistry, University of Southampton, Southampton SO17 1BJ, United Kingdom, and Department of Biochemistry, Wageningen Agricultural University, Dreijenlaan 3, 6703 HA Wageningen, The Netherlands

Received February 15, 2001; Revised Manuscript Received May 16, 2001

ABSTRACT: Cytochromes c_3 isolated from *Desulfovibrio* spp. are periplasmic proteins that play a central role in energy transduction by coupling the transfer of electrons and protons from hydrogenase. Comparison between the oxidized and reduced structures of cytochrome c_3 isolated from *Desulfovibrio vulgaris* (Hildenborough) show that the residue threonine 24, located in the vicinity of heme III, reorients between these two states [Messias, A. C., Kastrau, D. H. W., Costa, H. S., LeGall, J., Turner, D. L., Santos, H., and Xavier, A. V. (1998) *J. Mol. Biol. 281*, 719−739]. Threonine 24 was replaced with valine by site-directed mutagenesis to elucidate its effect on the redox properties of the protein. The NMR spectra of the mutated protein are very similar to those of the wild type, showing that the general folding and heme core architecture are not affected by the mutation. However, thermodynamic analysis of the mutated cytochrome reveals a large alteration in the microscopic reduction potential of heme III (75 and 106 mV for the protonated forms of the fully reduced and oxidized states, respectively). The redox interactions involving this heme are also modified, while the remaining heme−heme interactions and the redox−Bohr interactions are less strongly affected. Hence, the order of oxidation of the hemes in the mutated cytochrome is different from that in the wild type, and it has a higher overall affinity for electrons. This is consistent with the replacement of threonine 24 by valine preventing the formation of a network of hydrogen bonds, which stabilizes the oxidized state. The mutated protein is unable to perform a concerted two-electron step between the intermediate oxidation stages, 1 and 3, which can occur in the wild-type protein. Thus, replacing a single residue unbalances the global network of cooperativities tuned to control thermodynamically the directionality of the stepwise electron transfer and may affect the functionality of the protein.

The reduction potential of heme groups is modulated by several factors: the nature of the axial ligands to the heme iron, solvent accessibility, and interaction of the porphyrin ring substituents with neighboring groups such as charged residues or redox center(s) (*1*−*7*). The influence of the axial ligands on the reduction potential is due not only to the nature of those amino acid residues but also to their interaction with residues of the protein matrix, through hydrogen bonds (*7*). Mutations that affect heme exposure to the solvent indicate that the dielectric constant in the heme pocket is also an important factor in modulating the reduction potential (*4*). Furthermore, disruption of the hydrogen-bond networks involving the heme propionate groups and surrounding residues has been shown to cause alterations in the reduction potential of cytochromes (*8*). Site-directed mutagenic studies performed in *c*- and *b*-type cytochromes show that all of these factors contribute, to different extents, to poise the reduction potential of the heme group (*4*). Also, if a protein contains multiple redox groups, the potential of each redox center can be influenced by the redox state of the others (*9*−*11*). This is the case in cytochrome *c* oxidase, where interactions between redox groups are important to control the efficiency of its functional mechanism (*12*−*16*).

Lin et al. (*17*) studied the effect of adding or removing hydrogen bonds between the reaction center of *Rhodobacter sphaeroides* and the primary electron donor by site-directed mutations. The authors showed that significant changes in the midpoint potential occur, suggesting that the hydrogen bonds are extremely important in the tuning of the reduction potentials needed for electron transfer in *Rh. sphaeroides*. The importance of a conserved hydrogen-bonding network to the reduction potential for *Rhodobacter capsulatus* cyto-

† This work was supported by an EU grant (FMRX-CT-98-0218) and by a FCT-Portugal grant (PCTI/1999/BME/35021).

* Corresponding author: phone 351-214428616; fax 351-214428766; e-mail xavier@itqb.unl.pt.

‡ Instituto de Tecnologia Química e Biológica, Universidade Nova de Lisboa.

§ Faculdade Ciências e Tecnologia, Universidade Nova de Lisboa.

|| University of Southampton.

⊥ Present address: Structural & Computational Biology, European Molecular Biology Laboratory (EMBL), Meyerhofstrasse 1, D-69117 Heidelberg, Germany.

▽ Wageningen Agricultural University.

10.1021/bi010330b CCC: $20.00
Published on Web 07/18/2001

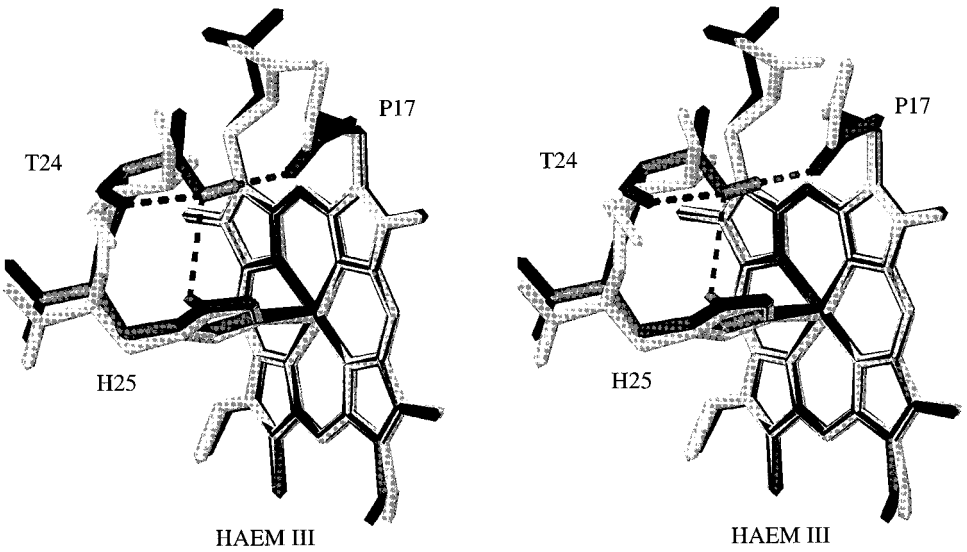

FIGURE 1: Stereoview of heme III, T24 and H25 of *Dv*Hc_3 in the reduced and oxidized form. The oxidized form (*30*) is shown in black and the reduced (*28*) in gray. The three hydrogen bonds established by T24 (between H^N and $O^{\gamma 1}$ of T24, between T24 $H^{\gamma 1}$ and one of the carboxyl oxygen atoms of heme III propionate 17, and between T24 $O^{\gamma 1}$ and $H^{\delta 1}$ of the heme III axial ligand, H25) in the oxidized state are also indicated by dashed lines.

chrome c_2 and cytochrome *c* peroxidase was also demonstrated by mutagenesis (*18, 19*). Recently, Xue et al. (*20*) and Sarma et al. (*21, 22*) mutated residues forming hydrogen bonds near the heme group of cytochrome b_5. The authors showed that mutations of these residues caused changes in the heme reduction potential in the range 21−27 mV. These variations were explained as a result of modifications in the hydrogen-bond network around the heme and in the coordination distances between the heme iron and the two axial ligands.

Desulfovibrio cytochromes c_3 are multihemic proteins, in which interactions between the four heme groups and neighboring residues result in homotropic redox cooperativity, the dependence of each heme reduction potential on the redox states of the other hemes, and heterotropic (redox−Bohr) cooperativity, the pH dependence of the heme reduction potentials. Due to their small size and monomeric structure, cytochromes c_3 are good models for studying the mechanisms of such cooperativities in biological systems. These mechanisms are probably of general importance to the metabolism of various bacteria since the presence of tetrahemic cytochromes has been detected not only in all *Desulfovibrio* species but also in other species, such as *Shewanella putrefaciens* (*23*) and *Shewanella frigidimarina* (*24, 25*). The structural basis of cooperativity in *Dv*Hc_3[1] has been investigated by site-specific mutagenesis (*26, 27*). These studies supported the identification of a lysine residue in modulating the pK_a of heme I propionate groups (*28*), thereby controlling the pH dependence of the heme I reduction potential (redox−Bohr effect) through redox-linked modifications of the K45/propionate interactions previously predicted by theoretical studies (*29*). This localized rearrangement in the vicinity of the propionate groups of heme I, which involves the covalent linkage of heme II (C46), is also consistent with the positive cooperativity (negative redox energies) governing a coordinated two-electron step (*28*). Together, the positive redox−Bohr effect and the positive redox cooperativity between hemes I and II explain the effect of cytochrome c_3 in stimulating hydrogenase activity ($H_2 \rightarrow 2H^+ + 2e^-$) (*11*).

Structures for the oxidized and reduced forms of *Dv*Hc_3 have been obtained by X-ray (*30, 31*) and NMR (*28*), respectively. One of the most striking differences between the two forms concerns the reorientation, upon reduction, of the side chain of T24, a residue located near heme III. This reorientation results in the breakage of three hydrogen bonds established by T24 in the oxidized state: between H^N and $O^{\gamma 1}$ of T24, between T24 $H^{\gamma 1}$ and one of the carboxyl oxygen atoms of heme III propionate 17, and between T24 $O^{\gamma 1}$ and $H^{\delta 1}$ of the heme III axial ligand, H25 (*28*) (Figure 1). In *Desulfovibrio gigas* cytochrome c_3 the homologous residue T28 undergoes a similar redox-linked reorientation in solution (*32*). To investigate the effect of this redox-linked conformational change on the general redox properties of *Dv*Hc_3, T24 was replaced by the nonpolar residue valine, and the thermodynamic properties of the mutated cytochrome were analyzed. This analysis shows how T24 and homologous residues can control the redox properties of tetraheme cytochromes.

MATERIALS AND METHODS

Site-Directed Mutagenesis. The T24V mutation was introduced in the gene encoding *Dv*Hc_3, cloned in plasmid pJ800 (*33*), by use of the QuickChange site-directed mutagenesis kit (Stratagene) and synthetic oligonucleotides purchased from Life Science Technologies. The mutation was confirmed by nucleotide sequencing.

Nucleotide Sequencing. The nucleotide sequence was checked by the dideoxy chain-terminator method (*34*), using the Thermo Sequenase cycle sequencing kit (Amersham), synthetic oligonucleotides purchased from Gibco−BRL, and the proofreading DNA polymerase *Pfu* (Stratagene). The restriction endonucleases and [α-^{35}S]dATP were purchased from Roche Molecular Biochemicals and from Amersham, respectively.

[1] Abbreviations: *Dv*Hc_3, *Desulfovibrio vulgaris* (Hildenborough) cytochrome c_3; NOESY, nuclear Overhauser enhancement spectroscopy; *Dd*27c_3, *Desulfovibrio desulfuricans* 27774 cytochrome c_3.

Bacterial Growth and Purification of T24V Mutated Protein. Mutated cytochrome c_3 was produced in *Desulfovibrio desulfuricans* G200 by use of the broad-host-range vector pJRD215, as described previously (*26*, *27*). The mutated *Dv*Hc_3 was then purified as described by Saraiva et al. (*26*).

Visible Redox Titration. Anaerobic visible redox titrations were performed as described previously (*11*), with ca. 2 μM protein solutions in 50 mM Tris-HCl buffer at pH 6.5 and 8.2. A solution of the following redox mediators (indigo tetrasulfonate, indigo trisulfonate, indigo disulfonate, 2-hydroxy-1,4-naphthoquinone, anthraquinone-2,7-disulfonate, phenosafranine, safranine O, neutral red, diquat, and methylviologen) was added to the protein solution to give final concentrations of 1 μM. Visible spectra were recorded in a Shimadzu UV-360 spectrophotometer.

NMR Spectroscopy. For the NMR studies, 2 mM protein samples were prepared as previously described (*26*). Two-dimensional spectra were recorded at 298 K in a 500-MHz Bruker DRX-500 spectrometer. In the intermediate states of oxidation, the NOESY experiments were performed at several pH values with mixing times of 25 ms, data size 512 $\times$ 2048, and spectral width of 33 kHz. NOESY spectra for the fully reduced and oxidized states were acquired with 100 and 20 ms mixing times, respectively. To allow comparison with the wild-type NMR data, the NOESY spectrum of the reduced mutated cytochrome was acquired at 303 K, pH 8.5, data size of 1K $\times$ 4K, and a spectral width of 8 kHz. Similarly, in the fully oxidized protein, the NOESY spectrum was acquired at 303 K, pH 7.1, data size of 1K $\times$ 4K, and a spectral width of 17.5 kHz. Chemical shifts are presented in parts per million (ppm) relative to sodium 3-(trimethylsilyl)[2,2,3,3-$^2H_4$]propanesulfonate, with tris-(hydroxymethyl)aminomethane ($C_4H_{11}NO_3$) as an internal reference.

Modeling. The simplest model that can describe the thermodynamic properties of *Dv*Hc_3 considers five interacting centers: four hemes and one ionizable center (*11*, *35*). Since *Dv*Hc_3 exhibits fast intramolecular and slow intermolecular electron exchange on the NMR time scale, any heme substituent displays five discrete NMR signals corresponding to each of the five possible macroscopic oxidation stages, connected by four one-electron steps. Thus, the paramagnetic shifts of heme substituents can be used to obtain the relative microscopic reduction potentials of the heme groups in each stage of oxidation (*10*, *11*, *36*). However, the paramagnetic shift observed for a particular heme substituent depends not only on the Fermi contact and the dipolar contributions of its own heme (intrinsic shift) but also on the dipolar shift due to the other hemes (extrinsic shift) (*36*−*38*). Therefore, the paramagnetic shift observed for a heme substituent is directly proportional to its fractional oxidation only in the absence of an extrinsic contribution. As shown previously for *Dv*Hc_3 (*38*), the heme methyl groups $18^1CH_3^I$, $18^1CH_3^{II}$, $12^1CH_3^{III}$, and $18^1CH_3^{IV}$ (Roman numbers designate the heme order in the polypeptide chain) have large paramagnetic shifts and negligible extrinsic dipolar contributions; hence they are suited to monitor the thermodynamic properties of this cytochrome.

Since the NMR data provide only relative reduction and heme interaction potentials (*10*, *11*, *35*, *39*), it is necessary to calibrate these values with redox titrations, monitored by visible spectroscopy. The computer program used in this work fits the five center thermodynamic model, referred to above, to the NMR and visible data sets simultaneously (*40*). The half-height widths of the NMR signals were used as a measure of the uncertainty of each chemical shift. Experimental errors of $\pm$2% were assumed for the visible data points.

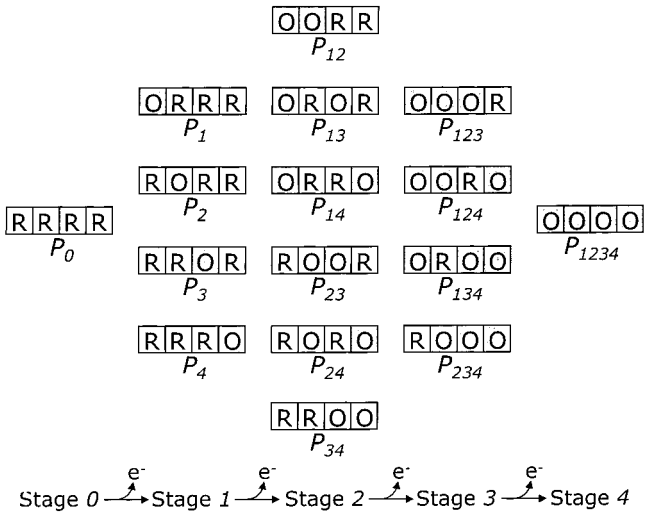

FIGURE 2: Diagram of the 16 populations that correspond to the five redox stages connected by one electron step. The redox stages are numbered 0−4 from the fully reduced to the fully oxidized states. The intramolecular electron exchange (within the same oxidation stage) is fast whereas the intermolecular electron exchange (between different oxidation stages) is slow on the NMR time scale. The boxes represent the four different hemes, which can be either reduced (R) or oxidized (O) and placed accordingly to their position in the polypeptide chain. Each population (*P*) represents the sum of the protonated and deprotonated form of a single pair of microstates, labeled according to the oxidized heme(s).

The process of fitting the thermodynamic parameters involves adjusting the energies, and hence the populations, of the 32 microstates in which each of the four hemes is oxidized or reduced and the ionizable center is protonated or deprotonated (*11*). Since proton exchange is fast on the NMR time scale, the properties of the hemes are represented by the population of pairs of microstates, which we label in the next section with the numbers of those hemes that are oxidized in each case. Thus, for example, stage 4 represents the fully oxidized protein, which comprises a single pair of microstates with the population label P_{1234} (cf. Figure 2).

RESULTS AND DISCUSSION

Compared with the wild-type cytochrome, the overexpressed T24V*Dv*Hc_3 showed no detectable differences in yield, stability, or optical properties. Furthermore, the analysis of 2D-NMR NOESY spectra of the fully reduced and oxidized forms of this cytochrome shows that the mutation did not alter the architecture of the tetraheme core. In fact, the network of interheme NOE cross-peaks is essentially equivalent to that described for the wild type (*38*, *41*).

The NMR redox titrations show that, as in the native cytochrome (*36*), the mutated protein exhibits fast intramolecular and slow intermolecular electron exchange (Figure 2). The same set of heme methyl groups ($18^1CH_3^I$, $18^1CH_3^{II}$, $12^1CH_3^{III}$, and $18^1CH_3^{IV}$) used to obtain the redox parameters of the wild-type cytochrome (*11*, *38*) was used to monitor the thermodynamic properties of T24V*Dv*Hc_3.

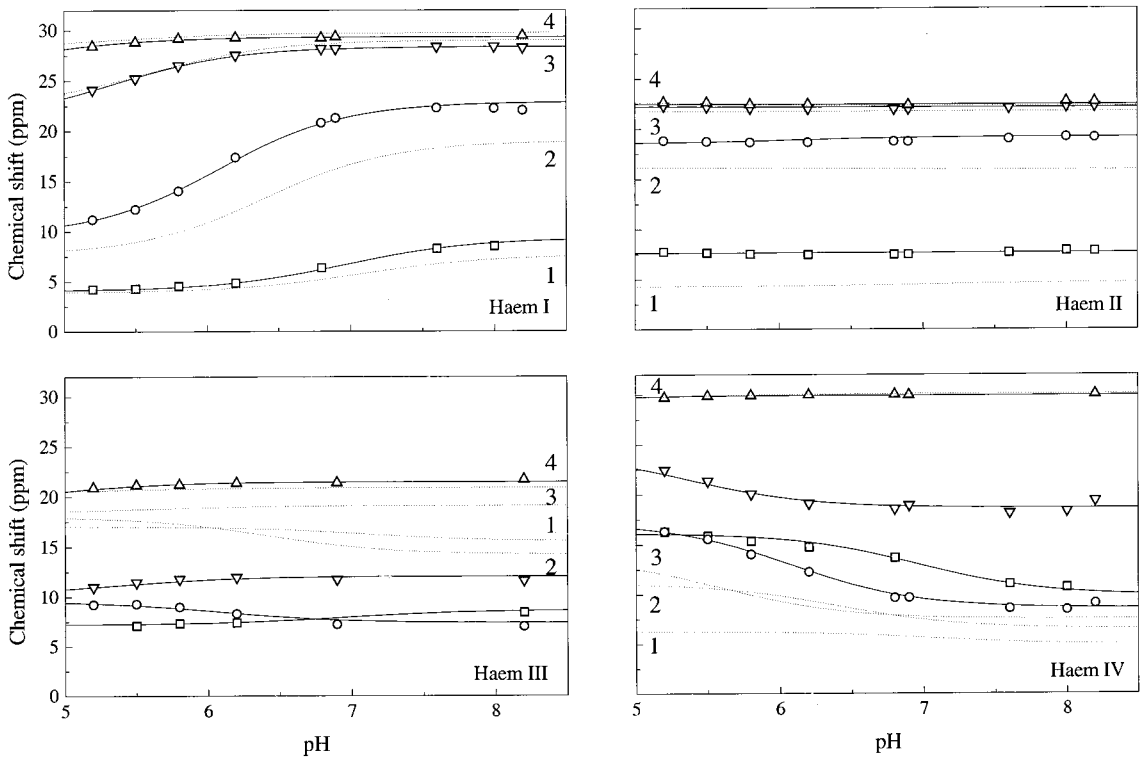

FIGURE 3: pH dependence of the chemical shift of heme methyl group resonances $18^1CH_3^I$, $18^1CH_3^{II}$, $12^1CH_3^{III}$, and $18^1CH_3^{IV}$, of the mutated cytochrome at 298 K. (□) Stage 1 of oxidation; (○) stage 2; (▽) stage 3; (△) stage 4. The chemical shifts of the heme methyl groups in the fully reduced stage 0 are not plotted since they are unaffected by the pH. They are 3.32 ($18^1CH_3^I$), 3.13 ($18^1CH_3^{II}$), 3.49 ($12^1CH_3^{III}$), and 3.32 ($18^1CH_3^{IV}$) ppm for the mutated cytochrome and 3.30 ($18^1CH_3^I$), 3.13 ($18^1CH_3^{II}$), 3.44 ($12^1CH_3^{III}$), and 3.29 ($18^1CH_3^{IV}$) ppm for the wild-type cytochrome. The full lines represent the best fit of the shifts for the mutated cytochrome to the model of five interacting centers using the energy parameters listed in Table 2. Dashed lines represent the best fit for the wild-type cytochrome and the nearest label (1−4) indicates the oxidation stage indicated by the curve.

Table 1: Calculated Oxidation Fractions, X_i, for Each Heme Group in Each Oxidation Stage at pH 7.0 and 298 K for the Mutated and Wild-type Cytochromes[a]

oxidation stage	X_i			
	heme I	heme II	heme III	heme IV
0	0.00 (0.00)	0.00 (0.00)	0.00 (0.00)	0.00 (0.00)
1	0.13 (0.09)	0.23 (0.07)	0.25 (0.74)	0.36 (0.09)
2	0.70 (0.51)	0.83 (0.67)	0.23 (0.66)	0.23 (0.16)
3	0.96 (0.96)	0.98 (0.97)	0.47 (0.90)	0.58 (0.17)
4	1.00 (1.00)	1.00 (1.00)	1.00 (1.00)	1.00 (1.00)

[a] The oxidation stages are numbered from 0 (fully reduced) to 4 (fully oxidized), accordingly to the number of oxidized hemes. Values indicated in parentheses are those for the wild-type cytochrome.

Although chemical shifts of the fully reduced and oxidized forms of *Dv*Hc_3 and T24V*Dv*Hc_3 are closely similar, the paramagnetic shifts of T24V*Dv*Hc_3 heme methyl groups in the intermediate oxidation stages are quite different. This is particularly striking for heme methyl groups $12^1CH_3^{III}$ and $18^1CH_3^{IV}$ (Figure 3). The observed differences in the oxidation pattern results from a drastic change in the oxidation fraction of these two hemes, across the full pH range (5.2−8.2). The change in the pattern of oxidation fractions is exemplified at a single pH value in Table 1, at which hemes III and IV clearly show the largest variation from the wild-type protein.

The pH dependence of the paramagnetic shifts of these four heme methyl groups was fitted in the pH range 5.2−8.2, together with data obtained at pH 6.5 and 8.2 from visible spectroscopy, to the model of five interacting centers (see Materials and Methods). The result of this fitting is shown in Figure 3 and the thermodynamic parameters are listed in Table 2.

The change in the oxidation fractions is also evident from the comparison of the computed curves that describe the oxidation of individual hemes as a function of the solution potential (Figure 4A,B). As expected from the existence of redox interactions between the hemes, the curves are non-Nernstian (i.e., the value of *n*, number of electrons in the Nernst equation, differs from 1 and is not constant throughout the redox titration). Thus, the redox interactions allow the curves to cross over during the redox titration. Nevertheless, their apparent midpoint reduction potentials, $E^{0'}_{app}$ (i.e., the point at which the oxidized and reduced fractions are equally populated) can be used to indicate the order of heme oxidation (*11*). The substitution of T24 by a valine causes an alteration of the relative $E^{0'}_{app}$ values and a different order of overall oxidation is observed for the hemes: while in *Dv*Hc_3 the first heme to reach 50% oxidation is heme III, followed by hemes II, I, and IV (*36*, *42*), the relative order of oxidation of hemes II, I, and IV is maintained in T24V*Dv*Hc_3 but heme III becomes the last one to reach 50% oxidation. Indeed, the thermodynamic parameters determined for T24V*Dv*Hc_3 (Table 2) show that the microscopic reduction potential of heme III in stage 0 increases by 75 mV.

The individual heme redox interactions are not so strongly affected. In particular, the large positive cooperativity between hemes I and II remains unaltered and explains why these two heme groups still oxidize in a cooperative way ($n > 1$), and before hemes IV and III, despite the fact that the two hemes have a higher degree of oxidation in the first

Table 2: Thermodynamic Parameters Determined for *Dv*Hc_3 (*11*) and T24V*Dv*Hc_3[a]

	energies (meV)				
	heme I	heme II	heme III	heme IV	ionizable center
*Dv*Hc_3					
heme I	**−245 (−272)**	−43	20	−4	−70
heme II		**−267 (−310)**	−8	8	−30
heme III			**−334 (−290)**	32	−18
heme IV				**−284 (−248)**	−6
ionizable center					**439 (315)**
T24V*Dv*Hc_3					
heme I	**−209 (−208)**	−41	31	11	−80
heme II		**−258 (−281)**	4	14	−32
heme III			**−259 (−184)**	40	−36
heme IV				**−277 (−212)**	−14
ionizable center					**443 (281)**

[a] The thermodynamic parameters were determined by using a model of five interacting centers fitted to the NMR and visible data (see Material and Methods). Diagonal terms (in boldface type) represent the oxidation energies of the four hemes and the deprotonating energies for the ionizable center (standard errors of ca. 5 meV) in the fully reduced and protonated protein. The off-diagonal elements represent the redox and redox−Bohr energies between the five centers (standard errors of ca. 3 meV). The values in parentheses give the correspondent microscopic values for the fully oxidized state.

oxidation step (Table 1 and Figure 4A,B). Nevertheless, there is an increase of 31 mV in the sum of the reduction interacting potentials involving heme III as the others become oxidized. The increase in the microscopic reduction potential of heme III makes it similar to those of the other hemes in stage 0, but the oxidation of the other hemes (which have redox coupling with heme III of 31, 4, and 40 mV, respectively for hemes I, II, and IV) results in heme III having the highest $E^{0'}_{app}$. Thus, the reduction potential of heme III is more negative than those of the other three hemes in the wild-type cytochrome. This is not the case in T24V*Dv*Hc_3 (cf. Table 2); hence, P_3 clearly dominates the population of the first oxidation step in the wild-type cytochrome, but the populations of all four microstates in mutated cytochrome are similar in this oxidation step (cf. Figure 4 panels E and F). This behavior has an important effect on the oxidation profile of heme III at neutral pH (cf. Figure 4 panels A and B). Indeed, the oxidation curve of heme III in *Dv*Hc_3 is well separated from those of the other hemes at low solution potentials, i.e., in the early stages of oxidation (Figure 4B), but it only reaches full oxidation after hemes II and I due to the influence of its redox interactions. Since hemes II, I, and IV are only slightly oxidized at low solution potentials, the reduction potential of heme III is readily affected only in the latter part of its oxidation curve, when the other hemes become significantly oxidized. The redox interactions lead to a crossover of the oxidation curves so that hemes I, II, and III reach full oxidation almost at the same reduction potential, which is well separated from that of heme IV. This pattern is substantially altered in T24V*Dv*Hc_3. As mentioned above, in the mutated cytochrome all the hemes show similar percentages of oxidation at low solution potentials. Moreover, increasing the solution potential leads to the progressive oxidation of hemes I and II, which show a large percentage of oxidation when compared with heme III (Table 1 and Figure 4A). Thus, when heme III starts to be significantly oxidized, its reduction potential is strongly affected by the redox interactions with all the other oxidized hemes (Table 2). As a result, the oxidation curve of heme III is shifted from those of the other hemes in early stages of oxidation to higher reduction potential values (cf. Figure 4 panels A and B). Together, these effects lead to an increase of 106 mV in the microscopic reduction potential of heme III (in the acidic oxidized state) when compared with that in the wild type (Table 2).

The single mutation introduced (T24V) also produces important changes in the populations of the redox stages (cf. Figure 4 panels C and D) and in the relative population of the microstates (cf. Figure 4 panels E and F). In the mutated protein, the total population of the second oxidation stage (Figure 4C) is no longer smaller than those observed both for oxidation stages 1 and 3 as is the case in the wild-type protein (Figure 4D). Furthermore, although in *Dv*Hc_3 P_3 (heme III oxidized) dominates the populations of stage *1* (see above), in stage 2 (where two hemes are oxidized) the positive cooperativity between hemes I and II compensates for the initial difference between the reduction potentials of these two hemes and that of heme III. Thus, no single microstate dominates the populations of stage 2, and the global population of stage 2 is decreased, favoring a concerted two-electron step (between stages 1 and 3) performed by this protein (*42*). This is not the case in T24*Dv*Hc_3 (Figure 4C), where the similarity of all heme reduction potentials (see above) allows the interaction between heme I and II to dominate and generate a substantial population of the microstate P_{12} in oxidation stage 2. Thus, in T24*Dv*Hc_3 the two-electron step between the intermediate oxidation stages 1 and 3 is no longer favored.

Also, it becomes clear that the relative contributions of the different microstates to the overall population of each stage is dramatically changed (Figure 4E,F). While the dominant intermediate microstates of the oxidation stages 1, 2, and 3 in the *Dv*Hc_3 are P_3, P_{23} (although very small), and P_{123}, respectively, in T24V*Dv*Hc_3 the largest populations are P_4, P_{12}, and P_{124} (Figure 4E,F). The variation of the relative contribution of each microstate is even more striking. While in the wild-type cytochrome the population of stage 1 is clearly dominated by the microstate that has heme III oxidized, P_3 (Figure 4F), all four microstates, P_1-P_4, contribute significantly to the population of stage 1 in the mutant (Figure 4E). In oxidation stage 2 of T24V*Dv*Hc_3, the microstate with heme I and II oxidized, P_{12}, clearly dominates (Figure 4E). By contrast, all of the microstates have small populations at this oxidation stage in *Dv*Hc_3 (Figure 4F). Then, in oxidation stage 3 of *Dv*Hc_3, P_{123} is the main contributor to the population of stage 3 whereas two microstates, P_{124} and P_{123}, make significant contributions in T24V*Dv*Hc_3 (Figure 4E,F). Thus, whereas in *Dv*Hc_3 it is possible to define a route for the electrons ($P_0 \xrightarrow{e^-} P_3 \xrightarrow{2e^-} P_{123} \xrightarrow{e^-} P_{1234}$), there is no coherent path in T24V*Dv*Hc_3.

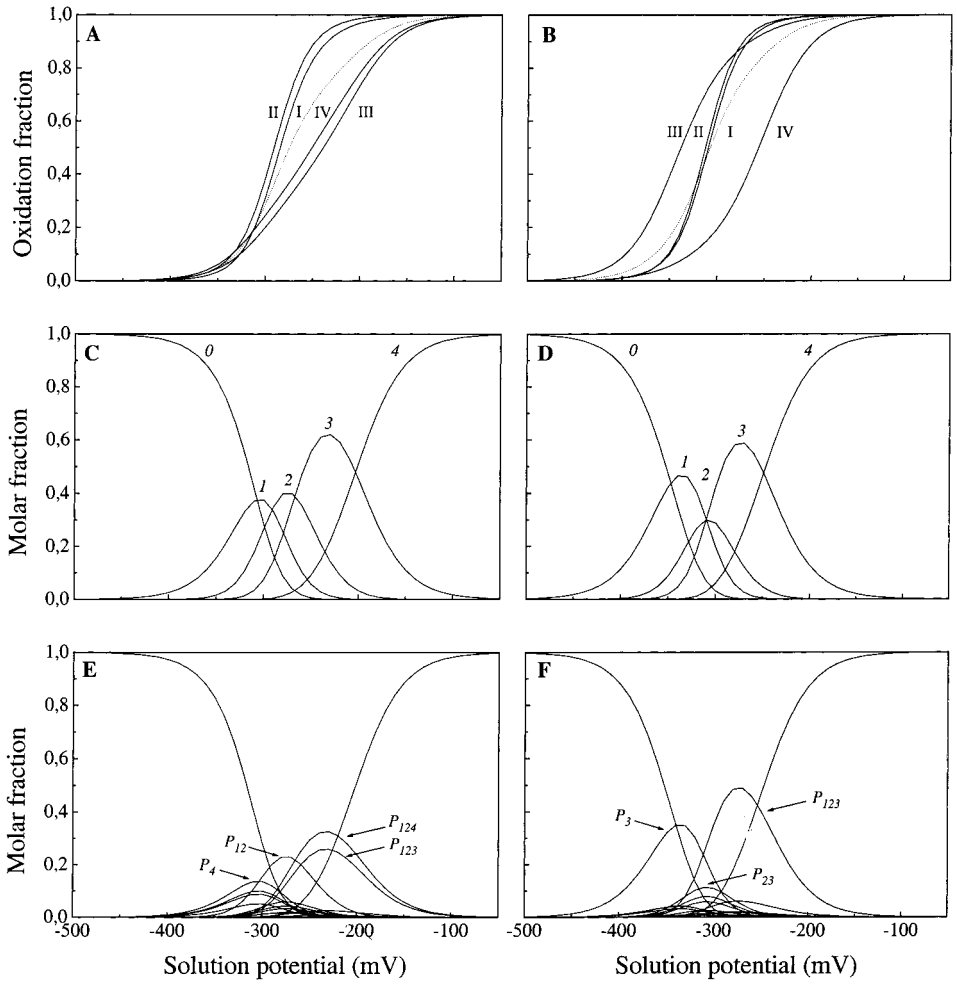

FIGURE 4: Oxidation states for the mutated and wild-type cytochromes at pH 7.0 and 298 K. The curves were calculated as a function of the solution reduction potential using the parameters listed in Table 2. The individual heme oxidation fractions (labeled with roman numerals) are shown in panels A and B for T24V*Dv*Hc$_3$ and *Dv*Hc$_3$, respectively together with the global oxidation fractions (dashed lines). The populations of the five redox oxidation stages (0−4) are plotted versus the solution reduction potential in panels C and D for T24V*Dv*Hc$_3$ and *Dv*Hc$_3$, respectively. Finally, the populations of the 16 pairs of microstates corresponding to the five redox stages are plotted versus the solution reduction potential in panels E and F for T24V*Dv*Hc$_3$ and *Dv*Hc$_3$, respectively. The dominant pair of microstates in each intermediate oxidation stages is labeled with the population P_{ijk} where *i*, *j*, and *k* represent the heme(s) oxidized in that particular microstate.

These results illustrate how a properly tuned network of cooperativities is fundamental to achieve an efficient two-electron step and reveal the importance of T24 in the electron-transfer mechanism of the wild-type cytochrome.

The thermodynamic analysis also provides the pK_a values for the different stages of oxidation (0−4): 7.5 (7.4), 7.0 (7.1), 6.1 (6.4), 5.3 (5.6), and 4.8 (5.3), with values in parentheses referring to the wild-type cytochrome. The alterations observed in the redox−Bohr interactions of the mutated protein are not substantial (Table 2), and the slight increase observed in the total redox−Bohr effect of the mutated cytochrome (0.7 pH unit) with respect to the wild type is largely due to a decrease of 18 mV in the redox−Bohr interaction of heme III (Table 2). In T24V*Dv*Hc$_3$, differences caused near heme III by the mutation could be responsible for this small variation, through the modulation of the dielectric constant or movement of the ionizable group. Previous work showed that the redox−Bohr effect in *Dv*Hc$_3$ is controlled by heme I propionates and neighboring residues (*11*, *27*, *28*), and since the residue mutated is not located close to heme I, the four macroscopic reduction potentials have a similar pH dependence in both cytochromes, although it is shifted to significantly higher values in T24V*Dv*Hc$_3$ (Figure 5).

Overall, the oxidation curve of the mutated cytochrome is shifted to higher potentials ($E^{0'}_{app} = -276$ mV), when compared with the wild-type protein ($E^{0'}_{app} = -306$ mV), making the mutant cytochrome more difficult to oxidize (Figure 4A,B). This is consistent with a relative destabilization of the oxidized state of the protein since the replacement of T24 by valine prevents the formation of a network of hydrogen bonds that stabilizes the oxidized state of the wild type (*28*).

To rationalize the thermodynamic differences observed between the mutated and wild-type cytochromes, we sought to determine the extent of structural changes in the reduced protein. Comparison of the 20 ms NOESY spectrum of T24V*Dv*Hc$_3$ in the fully reduced form, at 303 K and pH 8.5 in ^2H_2O, with that obtained under identical experimental conditions for the wild-type cytochrome revealed that changes in chemical shift are essentially restricted to protons located near the mutation site. In fact, only heme I thioether methyl ($C8^2H_3^I$) and methine ($C8^1H^I$), H25 $H^{\epsilon 1}$ (sixth ligand of heme III), and N21 H^{β} protons show significant differences

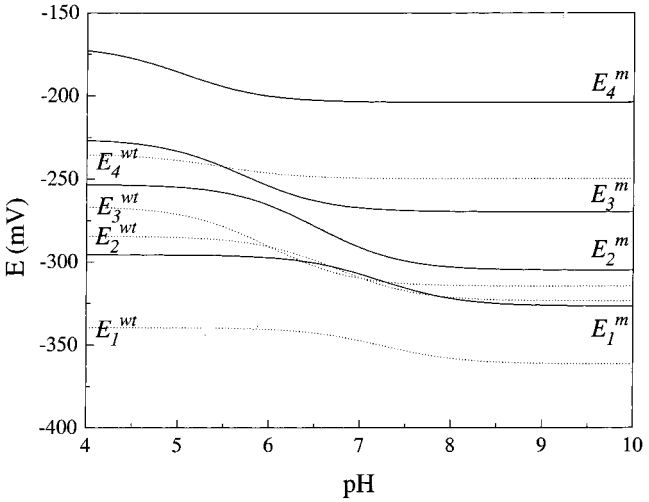

FIGURE 5: pH dependence of the four macroscopic reduction potentials for the T24V*Dv*Hc$_3$ and *Dv*Hc$_3$, at 298 K. The macroscopic reduction potentials were calculated from the parameters listed in Table 2. The solid and the dashed lines represent the macroscopic reduction potentials obtained for T24V*Dv*Hc$_3$ ($E_1^m - E_4^m$) and *Dv*Hc$_3$ ($E_1^{wt} - E_4^{wt}$), respectively. The labels on the right correspond to the solid lines, whereas those on the left correspond to the dashed ones.

Table 3: Proton Chemical Shifts[a] of the Assigned Signals That Show Larger Differences in the Fully Reduced Form of *Dv*Hc$_3$ and T24V*Dv*Hc$_3$ at 303 K and pH 8.5

protons	*Dv*Hc$_3$	T24V*Dv*Hc$_3$	difference
C8^{2}H3^I	0.35	−0.15	0.50
C8^{1}H^I	5.42	5.27	0.15
H25 H$^{\epsilon 1}$	1.63	1.26	0.37
N21 H$^{\beta}$	1.65	1.75	−0.10
	2.05	1.89	0.16

[a] Chemical shifts are given in parts per million.

in chemical shift, which are summarized in Table 3. The chemical shift variations observed have no simple explanation. Indeed, the change in the chemical shift of H25 H$^{\epsilon 1}$ cannot be attributed to a change in the protonation state of this histidine since the chemical shift of H25 H$^{\delta 2}$ remains unaltered (cf. ref *43*). The NMR data obtained in the fully reduced and oxidized states also indicate that the heme core architecture is maintained and no significant chemical shift differences are observed, either for the heme III protons or for the protons of the sixth heme III axial ligand (H83). Moreover, the empirical relationship between the chemical shifts of heme methyl groups in the oxidized bishistidinyl hemes and the orientations of the heme axial ligands (*44*) shows that the ligand geometry is not significantly affected by the mutation (data not shown). The observed chemical shift differences could be due to slight local conformational changes involving one of the axial histidine ligands (H25) of heme III because the volume occupied by the side chain of a valine residue is 16% larger than that of a threonine (*45*) and the side chain of T24 is less than 5 Å from the axial H25 ring. Since the H25 H$^{\delta 1}$ proton forms a hydrogen bond with N21 carbonyl oxygen (*28*), this might also explain the chemical shift changes observed in N21 H$^{\beta}$ and in heme I thioether protons. The resonances of the V24 side chain in T24V*Dv*Hc$_3$ are predicted to lie in a crowded region of the spectrum and could not be observed directly in order to confirm that the side chain occupies the same space as T24. However, any changes in the local conformation of the protein are clearly very small and localized.

The comparison between the thermodynamic parameters of the wild-type and the mutated cytochrome clearly illustrates the importance of the polypeptide chain in the fine-tuning the redox behavior of proteins in general and cytochromes c_3 in particular, where it may have functional significance. Indeed, all the cytochromes c_3 studied to date showed a highly conserved heme core architecture (ref *46* and references therein) despite the low homology in their amino acid sequence. Nevertheless, the thermodynamic properties of *D. vulgaris*, *D. gigas*, and *D. desulfuricans* 27774 (*Dd*27) cytochromes c_3 are all quite different (*11*, *37*, *40*, *47*).

CONCLUSIONS

The results described in the present work show that T24 has an important role in the control of the redox equilibrium of the cytochrome c_3 from *D. vulgaris* (Hildenborough) by stabilizing the oxidized form of the native cytochrome by forming a network of hydrogen bonds near heme III. The main effect of replacing this residue by a valine is to make the microscopic reduction potential of heme III much more positive, so that the redox equilibrium is shifted toward the reduced protein. In fact, the replacement of threonine by a valine residue changes the oxidation pattern of the protein such that the individual heme oxidation curves resemble those of *Dd*27c_3 (*47*, *48*). This cytochrome c_3 is unique among those that have been thermodynamically characterized to date, since it exhibits sequential oxidation of two pairs of hemes and where heme III is the last to oxidize. Interestingly, *Dd*27c_3 is also the only cytochrome c_3 without a threonine in position 24 (*31*, *49*). However, the alteration of the network of cooperativities by a single artificial mutation in T24V*Dv*Hc$_3$ is not counterbalanced by the global network of cooperativities. Thus, the electrons are dispersed among several microstates in each oxidation stage and it is impossible to define a specific path for the electrons. This is not the case in the wild-type *Dd*27c_3, where the protein is designed to control a specific path for the flow of electrons thermodynamically, by contrast with the control by structural arrangement that Dutton and collaborators have shown to be operative in larger multiredox center proteins and redox protein complexes (*50*).

REFERENCES

1. Armstrong, F. A. (1997) *J. Biol. Inorg. Chem. 2*, 139−142.
2. Bertini, I., Gori-Savellini, G., and Luchinat, C. (1997) *J. Biol. Inorg. Chem. 2*, 114−118.
3. Gunner, M. R., Alexov, E., Torres, E., and Lipovaca, S. (1997) *J. Biol. Inorg. Chem. 2*, 126−134.
4. Mauk, A. G., and Moore, G. R. (1997) *J. Biol. Inorg. Chem. 2*, 119−125.
5. Náray-Szabó, G. (1997) *J. Biol. Inorg. Chem. 2*, 135−138.
6. Warshel, A., Papazyan, A., and Muegge, I. (1997) *J. Biol. Inorg. Chem. 2*, 143−152.
7. Zhou, H.-X. (1997) *J. Biol. Inorg. Chem. 2*, 109−113.
8. Dangi, B., Blankman, J. I., Miller, C. J., Volkman, B. F., and Guiles, R. D. (1998) *J. Phys. Chem. B 102*, 8201−8208.
9. Palmer, G., and Olson, J. S. (1980) in *Molybdenum and molybdenum-containing enzymes* (Conghlan, M., Ed.) pp 189−220, Pergamon Press, New York.
10. Santos, H., Moura, J. J. G., Moura, I., LeGall, J., and Xavier, A. V. (1984) *Eur. J. Biochem. 141*, 283−296.

11. Turner, D. L., Salgueiro, C. A., Catarino, T., LeGall, J., and Xavier, A. V. (1996) *Eur. J. Biochem. 241*, 723−731.
12. Blair, D. F., Ellis, W. R., Jr., Wang, H., Gray, H. B., and Chan, S. I. (1986) *J. Biol. Chem. 261*, 11524−11537.
13. Chan, S. I., and Li, P. M. (1990) *Biochemistry 29*, 1−12.
14. Babcock, G. T., and Wikstrom, M. (1992) *Nature 356*, 301−309.
15. Sharp, R. E., and Chapman, S. K. (1999) *Biophys. Biochem. Acta 1432*, 143−158.
16. Behr, J., Hichel, H., Mentele, W., and Hellwing, P. (2000) *Biochemistry 39*, 1356−1363.
17. Lin, X., Murchison, H. A., Nagarajan, V., Parson, W. W., Allen, J. P., and Williams, J. C. (1994) *Proc. Natl. Acad. Sci. U.S.A. 91*, 10265−10269.
18. Caffrey, M. S., Daldal, F., Holden, H. M., and Cusanovich, M. A. (1991) *Biochemistry 30*, 4119−4125.
19. Goodin, B., and McRee, D. E. (1993) *Biochemistry 32*, 3313−3324.
20. Xue, L.-L., Wang, Y.-H., Xie, Y., Yao, P., Wang, W.-H., Qian, W., and Huang, Z.-X. (1999) *Biochemistry 38*, 11961−11972.
21. Sarma, S., Dangi, B., Yan, C., DiGate, R. J., Banville, D. L., and Guiles, R. D. (1997) *Biochemistry 36*, 5645−5657.
22. Sarma, S., DiGate, R. J., Goodin, D. B., Miller, C. J., and Guiles, R. D. (1997) *Biochemistry 36*, 5658−5668.
23. Tsapin, A. I., Nealson, K. H., Meyers, T, Cusanovich, M. A., Beuumen, J. V., Crosby, L. D., Feinberg, B. A., and Zhang, C. (1996) *J. Bacteriol. 178*, 6386−6388.
24. Gordon, E. H. J., Pike, A. D., Hill, A. E., Cuthbertson, P. M., Chapman, S. K., and Reid, G. A. (2000) *Biochem. J. 349*, 153−158.
25. Pessanha, M., Brennan, L., Xavier, A. V., Cuthbertson, P. M., Reid, G. A., Chapman, S. K., Turner, D. L., and Salgueiro, C. A. (2001) *FEBS Lett. 489*, 8−13.
26. Saraiva, L. M., Salgueiro, C. A., LeGall, J., van Dougen, W. M. A. M., and Xavier, A. V. (1996) *J. Biol. Inorg. Chem. 1*, 542−550.
27. Saraiva, L. M., Salgueiro, C. A., da Costa, P. N., Messias, A. C., LeGall, J., van Dongen, W. M. A. M., and Xavier, A. V. (1998) *Biochemistry 37*, 12160−12165.
28. Messias, A. C., Kastrau, D. H. W., Costa, H. S., LeGall, J., Turner, D. L., Santos, H., and Xavier, A. V. (1998) *J. Mol. Biol. 281*, 719−739.
29. Soares, C. M., Martel, P. J., and Carrondo, M. A. (1997) *J. Biol. Inorg. Chem. 2*, 714−727.
30. Matias, P. M., Frazão, C., Morais, J., Coll, M., and Carrondo, M. A. (1993) *J. Mol. Biol. 234*, 680−699.
31. Simões, P., Matias, P. M., Morais, J., Wilson, K., Dauter, Z., and Carrondo, M. A. (1998) *Inorg. Chim. Acta 273*, 213−224.
32. Brennan, L., Turner, D. L., Messias, A. C., Teodoro, M. L., LeGall, J., Santos, H., and Xavier, A. V. (2000) *J. Mol. Biol. 298*, 61−82.
33. Voordouw, G., and Brenner, S. (1986) *Eur. J. Biochem. 159*, 347−351.
34. Sanger, F., Nicklen, S., and Coulson, A. R. (1977) *Proc. Natl. Acad. Sci. U.S.A. 74*, 5463−5467.
35. Turner, D. L., Salgueiro, C. A., Catarino, T., LeGall, J., and Xavier, A. V. (1994) *Biochim. Biophys. Acta 1187*, 232−235.
36. Salgueiro, C. A., Turner, D. L., Santos, H., LeGall, J., and Xavier, A. V. (1992) *FEBS Lett. 314*, 155−158.
37. Salgueiro, C. A., Turner, D. L., LeGall, J., and Xavier, A. V. (1997) *J. Biol. Inorg. Chem. 2*, 343−349.
38. Salgueiro, C. A., Turner, D. L., and Xavier, A. V. (1997) *Eur. J. Biochem. 244*, 721−734.
39. Coletta, M., Catarino, T., LeGall, J., and Xavier, A. V. (1991) *Eur. J. Biochem. 202*, 1101−1106.
40. Louro, R. O., Catarino, T., Turner. D. L., Piçarra-Pereira, M. A., Pacheco, I., LeGall, J., and Xavier, A. V. (1998) *Biochemistry 37*, 15808−15815.
41. Turner, D. L., Salgueiro, C. A., LeGall, J., and Xavier, A. V. (1992) *Eur. J. Biochem. 210*, 931−936.
42. Louro, R. O., Catarino, T., Salgueiro, C. A., LeGall, J., and Xavier, A. V. (1996) *J. Biol. Inorg. Chem. 1*, 34−38.
43. Bundi, A., and Wüthrich, K. (1979) *Biopolymers 18*, 285−297.
44. Turner, D. L. (2000) *J. Biol. Inorg. Chem. 5*, 328−332.
45. Chothia, C. (1975) *Nature 254*, 304−308.
46. Nørager, S., Legrand, P., Pieulle, L., Hatchikian, C., and Roth, M. (1999) *J. Mol. Biol. 290*, 881−902.
47. Louro, R. O. (1998) *Proton-thrusters: energy transduction performed by tetraheme cytochromes c_3 and its physiological relevance*, Ph.D. Thesis, Instituto de Tecnologia Química e Biológica, Universidade Nova de Lisboa, Lisbon, Portugal.
48. Louro, R. O., Pacheco, I., Turner, D. L., LeGall, J., and Xavier, A. V. (1996) *FEBS Lett. 390*, 59−62.
49. Magro, V., Pieulle, L., Forget, N., Guigliarelli, B., Petillot, Y., and Hatchikian, E. C. (1997) *Biochim. Biophys. Acta 1342*, 149−163.
50. Page, C. C., Moser, C. C., Chen, X., and Dutton, P. L. (1999) *Nature 402*, 47−52.

BI010330B